Real-Fluid Equilibrium Evaporation Model for Lagrangian-Eulerian Simulation of Sustainable Aviation Fuel Sprays at High-Pressure Gas-Turbine Conditions

Srinivasan, Navneeth ; Han, Austin ; Poblador Ibanez, J.; Nocivelli, Lorenzo; Yang, Suo

DOI
10.2514/6.2025-0742

Publication date
2025

Document Version
Final published version

Published in
Proceedings of the AIAA SCITECH 2025 Forum

AIAA SciTech Forum
6-10 January 2025, Orlando, FL
AIAA SCITECH 2025 Forum

10.2514/6.2025-0742

Real-Fluid Equilibrium Evaporation Model for Lagrangian-Eulerian Simulation of Sustainable Aviation Fuel Sprays at High-Pressure Gas-Turbine Conditions

Navneeth Srinivasan *[1], Austin Han†[2], Jordi Poblador-Ibanez‡[3], Lorenzo Nocivelli§[2], and Suo Yang ¶[1]
[1]*Department of Mechanical Engineering, University of Minnesota – Twin Cities, Minneapolis, MN 55455, USA*
[2]*Transportation and Power Systems Division, Argonne National Laboratory, Lemont, IL, 60439, USA*
[3]*Department of Maritime and Transport Technology, Delft University of Technology, Delft, 2628 CD, The Netherlands*

The implementation of Sustainable Aviation Fuels (SAFs) in current and future long-haul aircraft to replace fossil-based kerosene represents the main path towards the decarbonization goal of the U.S. aviation industry by 2050. A deep and comprehensive characterization of the behavior of these new synthetic biofuels is a key to fulfill the strict regulations and standards and to ensure compatibility with existing propulsion systems in terms of performance, emissions, and safety. The present work focuses on the development of a Lagrangian-Eulerian thermodynamic framework to simulate SAF surrogates, employing the volume-translated Soave-Redlich-Kwong (VT-SRK) Equation of State (EoS) for accurate and efficient representation of thermodynamic properties. A novel computational fluid dynamics (CFD) solver, realFluidSprayFoam, was implemented within the OpenFOAM platform to account for high-pressure thermodynamics through real-fluid EoS-based departure functions and transport property corrections. This solver extends the application of real-fluid EoS to the Lagrangian phase, enabling precise modeling of multi-component liquid fuel mixtures via mixing rules. A new vapor-liquid equilibrium (VLE) based evaporation model of homogeneous droplets was developed and integrated into the solver to address the limitations of existing evaporation models, such as Raoult's law, under conditions near or beyond the critical point of SAFs. Validation was performed against microgravity experimental data for stationary heptane droplet evaporation at near- and super-critical conditions, demonstrating excellent agreement in evaporation curve slopes and droplet lifetimes. Further testing on multi-component SAF surrogates, showed strong agreement with high-fidelity Eulerian simulation data from the literature across various gas-turbine operating regimes. The preferential evaporation of volatile components and the corresponding impact on droplet lifetimes were effectively captured, highlighting the robustness and accuracy of the developed framework for high-pressure aerospace propulsion applications.

I. Introduction

Enabling the end-use of novel renewable fuels in the U.S. aviation sector is one of the pillars of the Sustainable Aviation Fuels (SAFs) Grand Challenge Roadmap*, which is a multi-agency initiative aimed at decarbonizing the aviation sector by 2050 by supplying sufficient SAFs to meet 100% of aviation fuel demand. SAFs are biofuels that offer net-zero carbon emissions during their life-cycle [1], and they are labeled as 'drop-in' if they are expected to replace traditional fossil-based kerosene (e.g., Jet A) in existing aviation propulsion systems. Despite this definition, it has been shown that drop-in SAFs may deviate from Jet-A behavior [2], especially in extreme conditions. This limits their current application only in blends up to 50% with Jet A and Jet A-1, as specified by the ASTM D4054 standard [3].

SAFs coming from different pathways - alcohol-to-jet (ATJ), Fischer-Tropsch (FT), hydroprocessed esters and fatty acids (HEFA), or power-to-liquid (PtL) processes - show a relatively simple composition spectrum, especially when compared with conventional jet fuels [2]. This feature enables the possibility of exploring the modeling of these fuels as

*Ph.D. Candidate, srini237@umn.edu (Corresponding Author), Student Member AIAA.
†Postdoctoral Appointee, Young Professional Member AIAA.
‡Postdoctoral Researcher, Young Professional Member AIAA
§Senior Research Scientist, Member AIAA.
¶Richard & Barbara Nelson Assistant Professor, suo-yang@umn.edu, Senior Member AIAA.
*https://www.energy.gov/eere/bioenergy/sustainable-aviation-fuel-grand-challenge

multi-component mixtures to increase the level of fidelity in the characterization of the fuels by common simplified surrogates available in literature [4–6]; thus, improving the computational fluid dynamics (CFD) workflow to simulate aerospace combustor systems. Models for thermophysical and transport properties of mixtures need to be compatible with the very broad operating range of aerospace combustors, which ranges from sub-atmospheric pressures and low temperatures typical of high-altitude relight conditions to supercritical regimes with extremely high pressures and temperatures at take-off and climb conditions [2].

The studies of trans-/super-critical injection and mixing, despite having attracted much interest in the past 30 years, have been concentrating on single-component systems, whose critical point is a constant value. As long as the fluid exceeds fuel's critical point, it is assumed to go into the supercritical state, and the classical "dense-fluid" approach is used with the assumption of a single phase [7]. Since the real mixture critical pressure could be significantly higher than the critical pressure of each component [8], the accurate mixture critical point needs to be obtained. The requirement for a thermophysical framework to capture the afore-motivated physical phenomena is achieved by using the vapor-liquid equilibrium (VLE) theory. The VLE theory enforces mechanical, thermal, and chemical equilibrium between the two phases, and hence estimates the phase fractions, phase densities, and phase compositions. Zhang et al. [9] showed details regarding the VLE-based CFD framework implementation. The VLE models were also incorporated into a reacting flow framework by Srinivasan et al. [10]. Zhang et al. [11] introduced an *in situ* adaptive tabulation (ISAT) model to alleviate computational costs associated with VLE calculations during CFD run time. Srinivasan et al. [12] introduced an artificial neural network (ANN) aided VLE model to tackle the robustness issues faced when integrating VLE into CFD solutions while also reducing the computational costs.

Due to the broad range of temporal and spatial timescales characteristic of combustors for aerospace application, resolving the liquid-gas interface becomes impractical, and therefore, the modeling community has been relying on Lagrangian-Eulerian approaches to model liquid injection and mixing with the gaseous flow [13, 14]. This framework describes the liquid phase as a cloud of discrete parcels [15], which are a statistical representation of the droplet distribution composing a spray, according to the discrete droplet model (DDM) by Dukovitz [16]. The trajectory of the parcels is tracked according to a Lagrangian approach coupled through two-way source terms with the carrier gas phase. The latter is defined within an Eulerian framework and discretized through a finite-volume scheme. The discontinuous nature of this representation of the two-phase flow and the impossibility to resolve droplet-scale physics force the usage of semi-empirical models to calculate source terms between parcels and gaseous cells.

The goal of this work is to define a physics-based robust cornerstone for the representation of the thermophysical properties of both phases, and to propose an upgrade of the conventional ideal-fluid evaporation sub-model that couples liquid and gaseous fields. The proposed framework aims to extend the accuracy of the two-phase flow model to higher pressures and temperatures, typical of realistic operation of aerospace combustors, and to improve the handling of multi-component mixtures. Some previous approaches have been proposed for different fuels and applications [17, 18], but no extensive analysis of the behavior of the evaporation of highly branched paraffins, typical of jet fuels, has been proposed or presented before.

The current paper provides an overview of the underlying models for the characterization of the thermophysical and transport properties of liquid and gas phases, showcases their implementation in a Lagrangian-Eulerian framework for CFD applications, which are discussed in Sec. II. Then validation against experimental data and comparison with higher-fidelity simulations for simplified test-cases are present in Sec. III and the findings are concluded in Sec. IV.

II. Numerical Methods

In this section, we summarize the fundamentals step taken to build a framework capable of capturing the non-ideal fluid behavior of hydrocarbons at elevated pressures and temperatures. The model is implemented in the open-source CFD code, OpenFOAM [19], and involves three major cornerstones: (a) definition of a comprehensive representation of real-fluid thermophysical and transport properties of liquid and gas species, (b) introduction of the real-fluid model in a Lagrangian-Eulerian spray application, and (c) implementation of a vapor-liquid equilibrium (VLE) dynamics to couple the two-phase.

A. Volume-Translated Soave-Redlich-Kwong (VT-SRK) Equation of State (EoS)

The relatively simple composition of SAFs motivates the implementation of a detailed real-fluid equation of state (EoS) framework to predict the properties of the fuel in liquid, gaseous, and supercritical phases as multi-component mixtures. Due to the need of computational efficiency to allow direct implementation of the EoS in CFD codes, we recently screened [20] the behavior of commonly used cubic EoS, i.e., the Soave-Redlich-Kwong (SRK) EoS [21] and

the Peng-Robinson (PR) EoS [22], to assess their performance in modeling the thermophysical properties of normal-, iso-, and cyclo-paraffins relevant for current aerospace biofuel candidates. These equations have been equipped with volume translation (VT) methods [23–25] to overcome their limitations in predicting density of compressed fluids [7, 26]. Their performance has been compared to NIST databases [27] and available experimental data [28].

The volume-translated (VT) formulation of a generalized equation of state (EoS) is shown in Eq. (1):

$$p = \frac{R_u T}{\overline{v} + c - b} - \frac{a}{(\overline{v} + c + \delta_1 b)(\overline{v} + c + \delta_2 b)}, \tag{1}$$

where R_u is the universal gas constant, $\overline{v}$ is the specific volume, δ_1 and δ_2 are constants specific to the selected EoS, a, b are functions of critical properties and acentric factor of the specific species in the mixture, and c is the volume translation (VT) coefficient calculated according to Lin et al. [23, 24]. Classical linear and quadratic mixing rules are implemented. The properties of the real fluid are determined following Poling et al. [29], which defines a departure function from the ideal state (given by *), dependent on the compressiblity factor Z and the molecular weight MW of the mixture. As an example, the formulation of the specific enthalpy h is given in Eq. (2):

$$h = h^* + \frac{R_u T}{MW}\left[(Z-1) + \int_{\infty}^{\overline{v}} T\left(\frac{\partial Z}{\partial T}\right)_{\overline{v}} \frac{d\overline{v}}{\overline{v}}\right]. \tag{2}$$

To determine the transport properties of species of interest, such as dynamic viscosity μ and thermal conductivity k, we used correlations valid for both liquid and gaseous fluid states according to the formulation by Chung et al. [30], which are defined as a function of pressure, temperature, density, and the physical properties of the species in the mixture. Further insight into the implementation of the real-fluid model (RFM) framework can be found in [20].

Very limited data is available in the literature for highly branched hydrocarbons relevant to SAFs, and uncertainty in their characterization in terms of molecular structure can affect the determination of inputs for EoS, namely critical pressure p_c, temperature T_c and specific volume v_c. In our approach, these input properties are derived assuming a probable structure of the molecule according to literature [31, 32] through group contribution methods using the formulation proposed by Nannoolal et al. [33], which also considers the normal boiling point T_b as an input. The acentric factor is determined according to the approach by Tahami et al. [34], and the dipole moment for viscosity and thermal conductivity correlations is defined as specified by Müller et al. [35]. The performance of the RFM against relevant pure species and mixtures using EoS variations can be found in Poblador-Ibanez and Nocivelli [20]. In this work, the VT-SRK implementation is shown as an acronym of volume-translated Soave-Redlich-Kwong equation of state, which proved to be the most consistent and accurate EoS implementation across the different candidates.

B. Real-Fluid Model based Lagrangian-Eulerian Solver

The required CFD solver to facilitate the simulation of aviation fuels with the appropriate EoS along with Lagrangian representation of the liquid phase was developed on OpenFOAM. The available default sprayFoam solver, which is a PIMPLE-based [36] low-Mach solver, was modified to account for multi-component mixture averaged transport and high-pressure thermodynamics, including a real-fluid EoS in the Eulerian phase.

The Chung's method [30] is used to evaluate the dynamic viscosity and thermal conductivity at high-pressure transcritical conditions. This method gives accurate calculations of viscosity and thermal conductivity of polar, non-polar, and associating pure fluids and mixtures [30]. Dynamic viscosity and thermal conductivity have a similar form given by

$$\lambda = \lambda_0 \lambda^* + \lambda_p, \tag{3}$$

where λ represents dynamic viscosity or thermal conductivity. λ_0 is the gas property at low pressures. λ^* and λ_p are high-pressure corrections. At high pressures, λ_p is the major contributing term compared to $\lambda_0\lambda^*$. At low pressures, λ^* approaches unity, and λ_p is negligible such that Eq. 3 reduces to λ_0. Hence, the transition between low and high pressures is smoothly described by the model.

For mass diffusivity, we use mixture-averaged mass diffusion model. The mass diffusion coefficient D_i of component i was defined by Kee et al. [37] as

$$D_i = \frac{1 - Y_i}{\sum_{j \neq i}^{N} X_j / D_{j,i}}, \tag{4}$$

where Y_i and X_i are the mass and mole fractions of the i-th component, respectively; $D_{i,j}$ is the binary diffusion coefficient, which is evaluated by Fuller's model [38] with Takahashi's correction for high pressures [39]. The thermodynamic and transport framework required for this application was built upon the work by Nguyen et al. [40].

The new solver included Lagrangian particles tracking, for which we modified the thermodynamic property estimation routines. In order to maintain consistency between the Eulerian (carrier) and Lagrangian (dispersed) phases, we replaced OpenFOAM's default polynomials fit to data available from standard references with the aforementioned EoS-based framework to estimate the required properties, such as density, thermal conductivity, viscosity, and mass diffusivity, etc. This updated workflow allowed us to model highly branched hydrocarbons, such as iso-paraffins with carbon number higher than 12, for which polynomials are not available as standard fuels. Furthermore, we improved the characterization of mixture properties by implementing real-fluid EoS-based mixing rules to replace the mole fraction-based weighted average mixing model conventionally used in OpenFOAM.

The implemented approach with a real-fluid EoS-based property estimation provides two major advantages. Firstly, poorly characterized fuels can still be represented using only EoS specific parameters, such as critical temperature and pressure, and do not require a large number of polynomial fits to represent them. Secondly, the implementation of mixing rules into the multi-component fuel droplets allows for accurate property estimation of multi-component fuels. We followed a modular approach in the definition of the solver - labeled realFluidSprayFoam - with its structure given in Fig. 1.

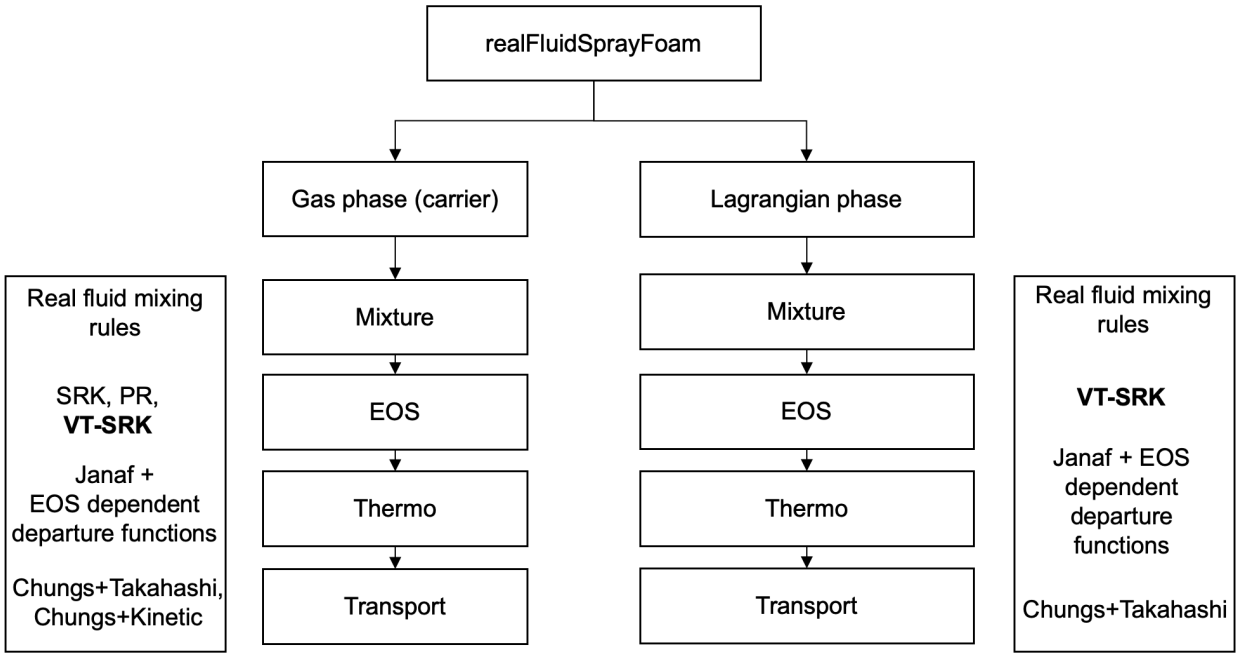

Fig. 1 Flowchart depicting the real-fluid based Lagrangian-Eulerian CFD solver model developed on OpenFOAM.

C. Vapor-Liquid Equilibrium (VLE) based Evaporation Model of Homogeneous Droplets

A new Lagrangian evaporation model is built upon the traditional Stefan-Fuchs (SF) formulation [41]. The SF model estimates the evaporating mass as shown in Eq. 5:

$$dm_i = \pi d_{drop} Sh_i D_i \rho \, log(1 + B_{M,i}) dt. \tag{5}$$

Here, subscript i indicates the i^{th} component/species in the Lagrangian droplet, d_{drop} is the droplet diameter, Sh_i is the Sherwood number of component i (estimated using the correlation in Eq. 6).

$$Sh_i = 2.0 + 0.6\sqrt{Re}\sqrt[3]{Sc_i}. \tag{6}$$

In order to estimate the Sherwood number Sh_i, the Reynolds number Re and the Schmidt number ($Sc_i = \nu/D_i$) are used to account for the flow/convective heat-transfer effects. D_i is the mixture-averaged diffusion coefficient of component i,

which can be estimated using high-pressure transport coefficient corrections described in Refs. [11, 12], and dt is the time-step size. $B_{M,i}$ is the Spalding mass transfer number of component i and is estimated by Eq. 7:

$$B_{M,i} = \frac{X_{i,s} - X_{i,c}}{1 - X_{i,s}}, \tag{7}$$

where $X_{i,c}$ represents the mole fraction of component i in the Eulerian carrier phase, and $X_{i,s}$ is the saturated vapor composition (i.e., the maximum allowed mole fraction of component i in the vapor phase for a given thermodynamic condition). The difference between the saturated state and the current state serves as a driving force for the vaporization process.

In the traditional SF model, $X_{i,s}$ is estimated using the Raoult's law [42], which uses the saturation pressure $P_{sat,i}$ of component i as described in Eq. 8:

$$X_{i,s} = X_{i,l} \frac{P_{sat,i}}{P}. \tag{8}$$

$X_{i,l}$ is the mole fraction of component i in the Lagrangian droplet, $P_{sat,i}$ is the saturation pressure of component i, and P is the mixture pressure. Raoult's law implies that the maximum partial pressure $PX_{i,s}$ of component i must be equal to the partial saturation pressure $P_{sat,i}X_{i,l}$ exerted by component i from the liquid phase. In other words, the saturation mole fraction $X_{i,s}$ is the required mole fraction in the vapor phase to attain vapor-liquid equilibrium (VLE). Raoult's law has been successful for modeling vaporization (especially for Lagrangian approaches) at low pressures, but often fails at high pressures (especially near critical points) [18]. Furthermore, Raoult's law does not account for multi-component effect, as no mixing rule is used while estimating saturation pressure $P_{sat,i}$ of an individual component i. Multi-component effects are significant at near-critical conditions [9]. To account for high-pressure and multi-component effects while imposing the VLE constraint, we utilize the real-fluid VLE theory with mixing rules.

To achieve VLE at high pressures, an approach based on the equality in fugacity – which can be seen as a real-fluid counter-part of partial pressure – for each individual component is necessary [11, 12]. The fugacities in the liquid and vapor phases of component i are expressed in Eqs. 9 and 10, respectively:

$$f_{i,L} = PX_{i,L}\phi_{i,L}; \tag{9}$$

$$f_{i,V} = PX_{i,V}\phi_{i,V}. \tag{10}$$

In Eq. 9 , P is the mixture pressure, $X_{i,L}$ is the mole fraction of component i in the Lagrangian liquid phase, and $\phi_{i,L}$ is the fugacity coefficient of component i in the Lagrangian liquid phase, which describes how much the fugacity $f_{i,L}$ deviates from its corresponding partial pressure $PX_{i,L}$. The similar terms are used to express fugacity of the vapor phase in Eq. 10.

The fugacity coefficient ϕ_i (Eq. 11) can be derived as a function of the equation of state (EoS) alone, and has been derived using the VT-SRK EoS:

$$ln(\phi_i) = \frac{Z + C - 1}{b}\left(\frac{\partial b}{\partial X_i}\right)_{X_{j\neq i}} - \frac{C}{c}\frac{\partial c}{\partial X_i}_{T,X_{j\neq i}} - ln(Z+C-B) - \frac{A}{(\delta_1 - \delta_2)B}\left(\frac{1}{a}\frac{\partial a}{\partial X_i}_{X_{j\neq i}} - \frac{1}{b}\frac{\partial ba}{\partial X_i}_{X_{j\neq i}}\right) ln\left(\frac{\overline{v} + c + \delta_1 b}{\overline{v} + c + \delta_2 b}\right). \tag{11}$$

The EoS parameters (a_i, b_i) of component i and mixture EoS parameters (a_p, b_p) are estimated using mixing rules, accounting for other active components. For the VT-SRK EoS, $\delta_1 = 1$ and $\delta_2 = 0$. More details are available in [20].

Imposing the fugacity equality between Eqs. 9 and 10, we can express $X_{i,V}$ as:

$$X_{i,s} = X_{i,V} = X_{i,L}\frac{\phi_{i,L}}{\phi_{i,V}}. \tag{12}$$

Here, we note that $X_{i,V}$ is the equilibrium mole fraction of component i in the vapor phase, which is also the definition of the saturation mole fraction $X_{i,s}$. Hence, we replace $X_{i,s}$ in Eq. 7 of the SF model with the the new formula of saturated vapor mole fraction derived in Eq. 12.

In addition, the vaporization rates are calculated using only the EoS parameters, and hence do not require any additional information, such as data fitted for saturation pressure $P_{sat,i}$ (required by traditional models such as Raoult's law) which is often available for traditional straight chained hydrocarbon fuels (in normal 'n' form) but often not available for branched hydrocarbon fuels (in 'iso' form). This implies that the current approach can also be used for surrogate fuels, especially when a single component/species is used to represent the entire fuel.

The flowchart of this model is depicted in Fig. 2, including the complete formulation. The addition of the critical temperature criterion ($T > T_c$) enables a full transition into a "supercritical" state (more precisely, either a supercritical state or a subcritical gaseous state, specifically for hydrocarbon fuels).

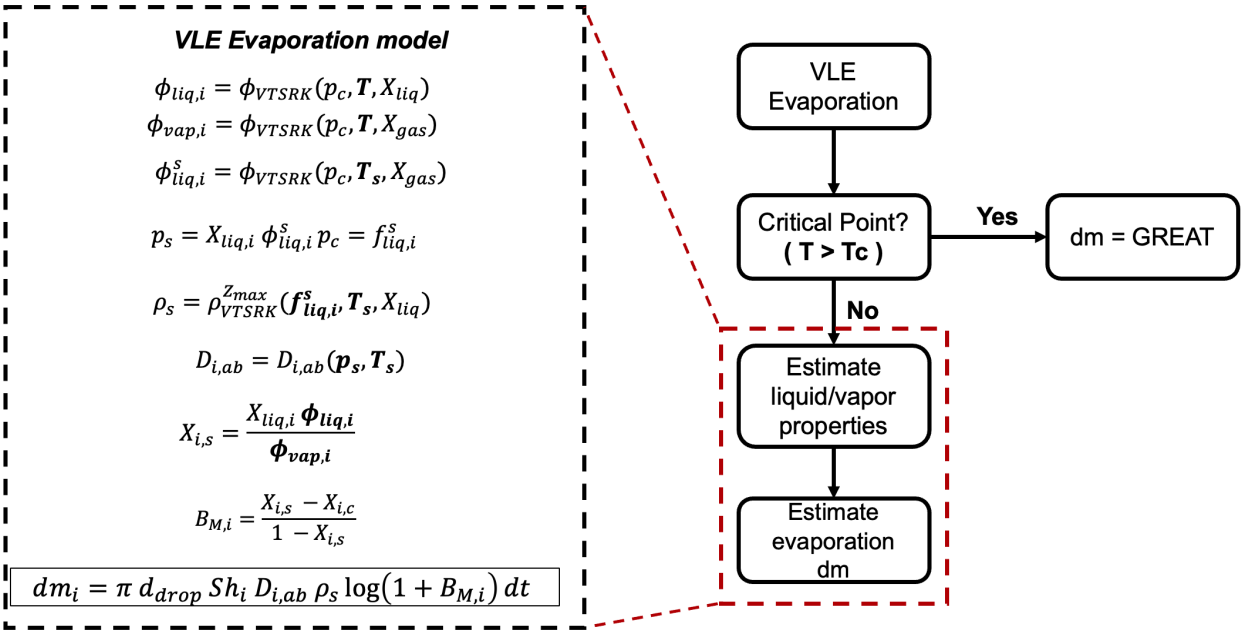

Fig. 2 Flowchart depicting the real-fluid VLE-based droplet evaporation model for Lagrangian-Eulerian (L-E) simulations. Critical temperature check ($T > T_c$) are included to identify whether the droplet has undergone "supercritical transition".

III. Results

A. Lagrangian Droplet Evaporation – n-heptane

In order to validate the developed model, a stationary Lagrangian droplet evaporation case was designed for evaporation of nC_7H_{16} in a quiescent N_2 atmosphere. This particular case is chosen to validate the model against experimental results of droplet evaporation in microgravity environments by Nomura et al. [43]. To evaluate the capabilities of the model, the conditions selected for validation are close to critical conditions of nC_7H_{16}. The case configuration is shown in Fig. 3. The droplet diameter is set to an initial value of 10 μm. To ensure accuracy and stability of the Lagrangian droplet evaporation case, the Eulerian mesh is designed to ensure that the volume fraction of the Lagrangian particle is no more than 10% (5-10% usually). Three operating conditions are chosen for validation, varying temperature and pressure as described in Table 1, where reduced temperature and pressure are defined as $T_r = \frac{T}{T_c}$ and $P_r = \frac{P}{P_c}$, respectively, referencing the critical conditions of pure nC_7H_{16} (T_c=546 K, P_c=27.4 bar). The focus of the validation is set on the capability of the model to capture the phase-change but not the initial heat-up of the liquid droplet, which might be affected by the difficulty of reproducing the experimental initial conditions. Therefore, the modeling data are aligned in time with the experiments, to provide the most accurate comparison in terms of droplet evaporation dynamics.

Table 1 Ambient temperature and pressure for droplet evaporation validation. Reduced temperature and pressure are defined as $T_r = \frac{T}{T_c}$ and $P_r = \frac{P}{P_c}$.

Case	Temperature [K]	Pressure [bar]	Reduced Temperature	Reduced Pressure
1	493	50	0.91	1.82
2	454	50	0.84	1.82
3	746	20	1.38	0.73

The simulation results and comparison against the experimental data by Nomura et al. [43] for Case 1 and Case 2 are shown in Fig. 4. Very good match is seen for Case 1 shown in Fig. 4a and good match is also seen for Case 2 in Fig. 4b during the first half of the evaporation period. Towards the end of the vaporization transient, which is longer due to

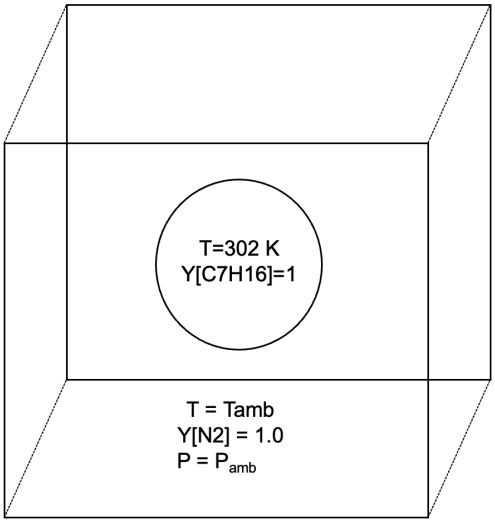

Fig. 3 Case configuration for nC_7H_{16} droplet evaporation into pure N_2 medium. Ambient temperature and pressure are described in Table 1.

the lower ambient temperature, the model diverges, and we ascribe this results to the underestimation of the fuel vapor fraction in the vicinity of the liquid-vapor interface. This effect is due to the instantaneous mixing of the vaporized mass with the gas in the cell surrounding the Lagrangian particle, which suppresses any species and temperature gradient outside of the liquid parcels, and determines a higher evaporation rate.

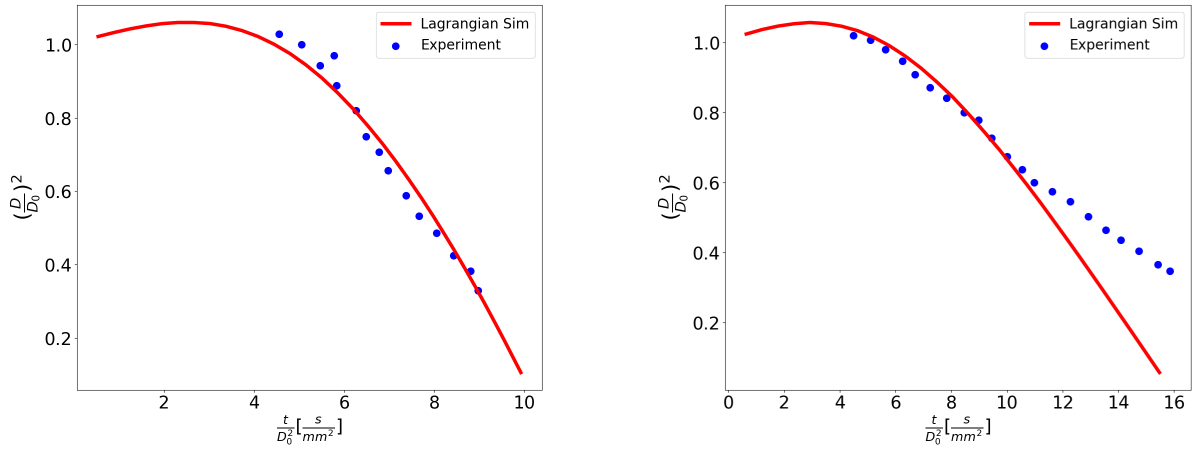

(a) T = 493 K, P = 50 bar, experimental data from Nomura et al. [43]

(b) T = 454 K, P = 50 bar, experimental data from Nomura et al. [43]

Fig. 4 Evaporation characteristics of nC_7H_{16} for Case 1 and CASE 2 vs. experimental data from Nomura et al. [43]

The behavior of the model in Case 3, where the ambient temperature is above the critical temperature of nC_7H_{16}, is shown in Fig. 5. When comparing the simulation results against the experimental results from Nomura et al. [43], we see good match in the initial stages of the evaporation, as shown in Fig. 5a, but we then see a difference between the simulated results and the experimental results. However, when comparing our results against numerical results for the same operating conditions from Zhang [44] and Poblador-Ibanez et al. [45] (simulated using a higher-fidelity Volume of Fluid, VoF, approach), we see a very good match with state-of-the-art Eulerian simulations.

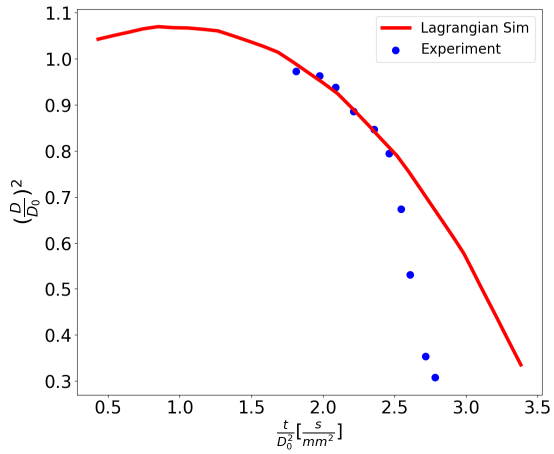

(a) T = 746 K, P = 20 bar, experimental data from Nomura et al. [43]

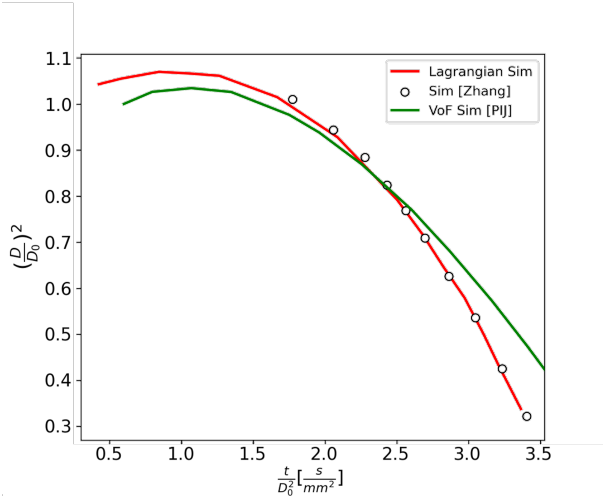

(b) T = 746 K, P = 20 bar. Simulations from [44] and [45]

Fig. 5 Evaporation characteristics of nC_7H_{16} for case 3 vs. experimental data from Nomura et al. [43] and numerical data from Zhang [44] and from Poblador-Ibanez et al. [45]

B. Lagrangian Droplet Evaporation – Two-component surrogate for NJFCP's C-1 test fuel

With the validation of the new model performed in the previous section, we proceed to test the new model against higher-fidelity Eulerian simulation results, obtained with a rigorous one-dimensional (1-D) model by Poblador-Ibanez et al. [45], for a multi-component stationary droplet evaporation representative of the C-type fuels proposed by the National Jet Fuel Combustion Program (NJFCP). Specifically, we chose to model C-1 [46], which represents the fuel conventionally labeled as POSF 11498. The ambient conditions were selected from certain operating zones (ORZ: outer recirculation zone, and CRZ: central recirculation zone) at relevant combustor conditions, as described in detail by Poblador-Ibanez et al. [45], and reported in Table 2.

Table 2 Thermophysical conditions of ambient and droplet for SAF surrogate droplet evaporation cases based on gas-turbine operating conditions. Conditions obtained from Poblador-Ibanez et al. [45] for central recirculation zone (CRZ) and outer recirculation zone (ORZ).

Case Name	Ambient Temperature [K]	Ambient Pressure [bar]	Droplet Temperature [K]	Diameter [μm]
Cruise - CRZ	1200	20	363	20
Cruise - ORZ	800	20	363	20
Takeoff - CRZ	1200	60	363	5
Takeoff - ORZ	900	60	363	5

We defined a simplified two-component surrogate to represent NJFCP's C-1 fuel, labeled C1ez, containing $iC_{12}H_{26}$ and $iC_{16}H_{34}$ as specified in Table 3.

Table 3 Fuel composition of surrogate fuel C1ez [20, 45].

	$iC_{12}H_{26}$	$iC_{16}H_{34}$
Mass Fraction	0.786	0.214

The evaporation characteristics simulated using the developed Lagrangian-Eulerian real-fluid solver and VLE-based Lagrangian evaporation model for the described two-component C1ez fuel are shown in Fig. 6. Good match is shown in the slope of the evaporation curve for all 4 conditions when compared to Poblador-Ibanez et al. [45]. Figure 6a depicts

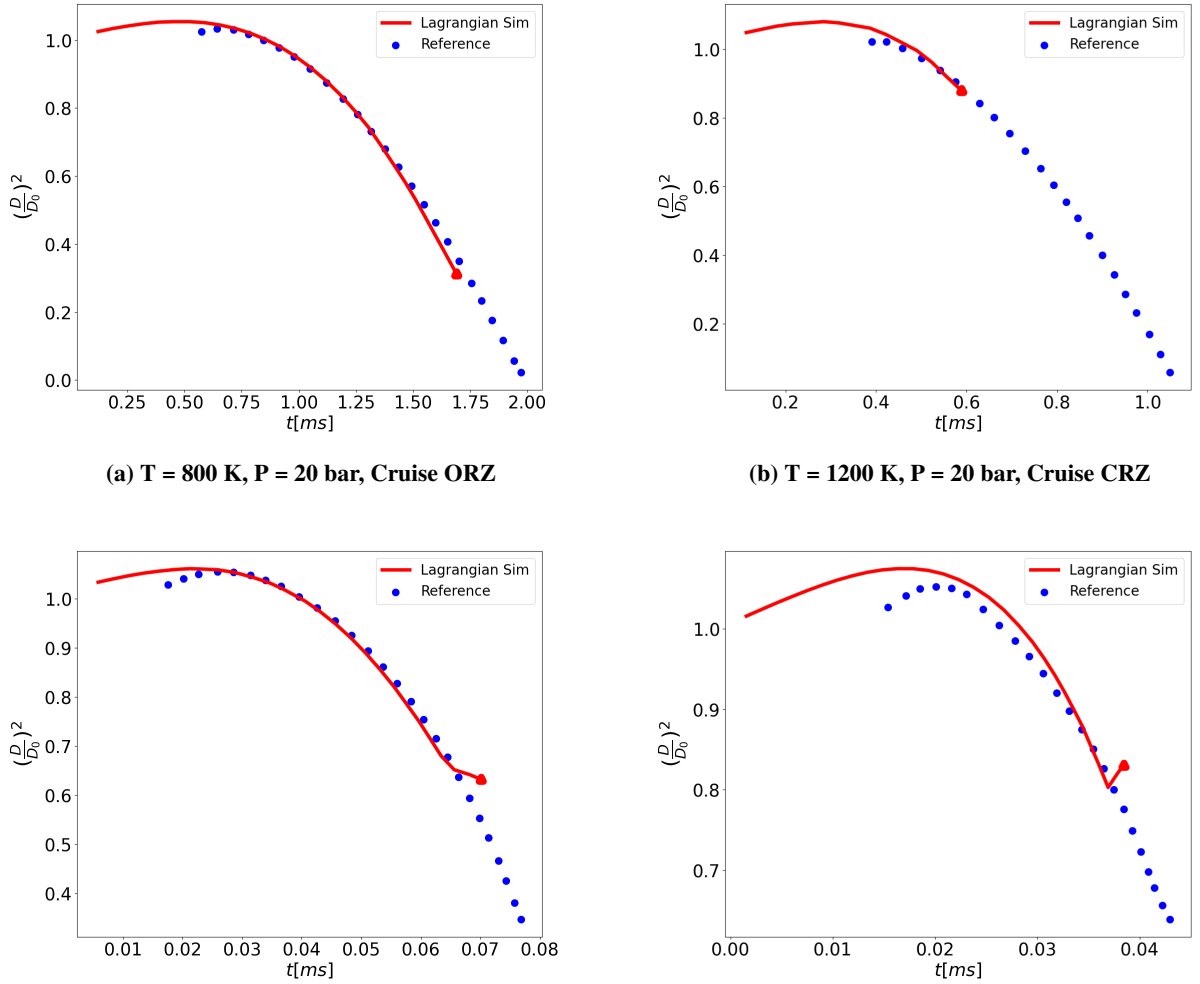

(a) T = 800 K, P = 20 bar, Cruise ORZ

(b) T = 1200 K, P = 20 bar, Cruise CRZ

(c) T = 900 K, P = 60 bar, Takeoff ORZ

(d) T = 1200 K, P = 20 bar, Takeoff CRZ

Fig. 6 Evaporation characteristics two-component SAF surrogate C1ez for operating conditions mentioned in Table 2. Comparison against data from Poblador-Ibanez et al. [45]. The 'red triangle' indicates "supercritical transition".

the cruise ORZ condition and shows very good match when comparing the slopes, whereas the cruise CRZ condition shown in Fig. 6b shows a good initial match but then predicts early "supercritical transition" (indicated by the red star). When looking at the take-off cases, both ORZ (Fig. 6c) and CRZ (Fig. 6d) show very good match for the evaporating slopes.

It is vital to note that Lagrangian formulation of liquids performs best in convecting cases where evaporation is driven by the convection correlations, and hence it is bound to face issues in stationary evaporation cases. Lagrangian parcels are modeled enforcing an infinitely rapid mixing of the components within the droplet (i.e., homogeneous droplet), and hence does not permit any species stratification and temperature gradients which can contribute to mismatches in the evaporation lifetime predictions. Therefore, given these underlying assumptions, we showcase the good performance of the two-component droplet evaporation against higher-fidelity and more expensive Eulerian simulation approaches.

C. Lagrangian Droplet Evaporation – Four-component surrogate for NJFCP's C-1 test fuel

One of the goals of multi-component modeling of fuels is to capture preferential evaporation, especially when large volatility differences exist between the fuel constituents. To study this impact, we simulate the evaporation characteristics

of a four-component surrogate of NJFCP's C-1 test fuel, labeled "C1", which consists of $iC_{12}H_{26}$, $iC_{13}H_{28}$, $iC_{16}H_{34}$ and $iC_{20}H_{42}$. Large differences in volatility are expected between $iC_{12}H_{26}$ and $iC_{20}H_{42}$ during evaporation transient. The mass fractions of the individual components in the surrogate fuel C1 are mentioned in Table 4.

Table 4 Fuel composition of surrogate fuel C1 [20, 45].

	$iC_{12}H_{26}$	$iC_{13}H_{28}$	$iC_{16}H_{34}$	$iC_{20}H_{42}$
Mass Fraction	0.802	0.018	0.163	0.017

The evaporation curves are shown in Fig. 7, alongside the variation of the composition of the liquid droplet. As seen in the figures, the evaporation slopes match the results from Poblador-Ibanez et al. [45] for all the operating conditions. However, droplet evaporation times are under-predicted by the Lagrangian model when compared to the Eulerain simulations from Poblador-Ibanez et al. [45]. This can be attributed to multiple effects, including rapid mixing assumption of the Lagrangian formulation leading to unavailability of spatial variations within the droplet and effects of the Eulerian mesh size on stationary droplet evaporation. However, as mentioned previously, the evaporation model proposed focused on the prediction of the slope of the evaporation, for which a good match is observed, even in the four-component case.

Figure 7 also shows the droplet composition (species mass fractions, which are modeled as uniform inside the droplet) during the evaporation for the four operating conditions. All four active species are shown. As expected, the lighter and hence more volatile component $iC_{12}H_{26}$ evaporates faster, leading to the increase in concentration of $iC_{16}H_{34}$, which is the other major component. The case where the complete extent of preferential evaporation is noted is the cruise-ORZ case, where competing preferential evaporation effects between $iC_{16}H_{34}$ and $iC_{20}H_{42}$ are seen. In the earlier stages of evaporation, the evaporated flux is dominated by $iC_{12}H_{26}$ leading to the increase in compositions of $iC_{16}H_{34}$ and $iC_{20}H_{42}$. As the process continues, a peak in $iC_{16}H_{34}$ composition is achieved, before its mass fraction starts to decrease and mass fraction of $iC_{20}H_{42}$ increases. Comparing this plot to the diameter plots, this peak is achieved in the last stages of the evaporation process and showcases the tendency of the less volatile compound to remain in the liquid phase and hence increase the droplet lifetime.

IV. Conclusions

The requirement for a Lagrangian-Eulerian thermodynamic framework to simulate Sustainable Aviation Fuel (SAF) surrogates was developed. The volume-translated Soave-Redlich-Kwong (VT-SRK) equation of state (EoS) was chosen to accurately and efficiently capture the thermodynamic properties of SAF surrogate fuels. Furthermore, a new Lagrangian-Eulerian computational fluid dynamics (CFD) solver, realFluidSprayFoam, was developed on the OpenFOAM platform, which accounts for high-pressure thermodynamics through real-fluid EoS and departure functions, and high-pressure transport properties through literature-based corrections. This solver also enabled the use of the real-fluid EoS-based framework in the Lagrangian phase, allowing for accurate descriptions of multi-component liquid fuel mixtures through the mixing rules of the real-fluid EoS.

Relevant operating conditions for aerospace combustors can reach the critical point of the injected fuels, and hence existing evaporation models which depend on Raoult's law fail to accurately capture the high-pressure evaporation. To accurately model the evaporation at these operating pressures, a new vapor-liquid equilibrium (VLE) droplet evaporation model was developed and integrated into the new solver. The new evaporation model, accounted for high-pressure effects through the fugacity coefficient estimated using the VT-SRK EoS. The fugacity can be viewed as the partial pressure equivalence at real-fluid operating conditions. The developed evaporation formulation utilizes the equilibrium condition of the VLE theory to estimate the saturated vapor concentration and the Spalding mass number, which is then used in the Stefan-Fuchs formulation to estimate the evaporative mass flux.

The developed model was validated against a set of experimental stationary nC_7H_{16} droplet evaporation cases conducted in microgravity environments. The validation was performed at near- and super-critical operating conditions defined with respect to nC_7H_{16}. Very good match of the evaporation curve 'slope' (i.e., the d^2 law) and droplet lifetime was seen, showcasing the accuracy of the developed Lagrangian droplet evaporation model. The model was further tested for multi-component surrogates of SAFs and the results were compared to previous higher-fidelity Eulerian simulations. The ambient conditions chosen were based on different operating regimes of a gas turbine which are near the critical point of the fuel. C1ez, a two-component SAF surrogate fuel, showed good match against the literature results. C1, a four-component surrogate fuel, also showed good match for the evaporation curve slope against literature.

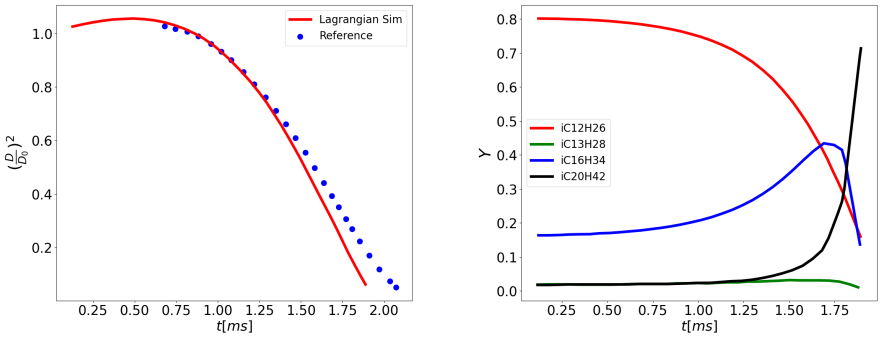

(a) T = 800 K, P = 20 bar, Cruise ORZ

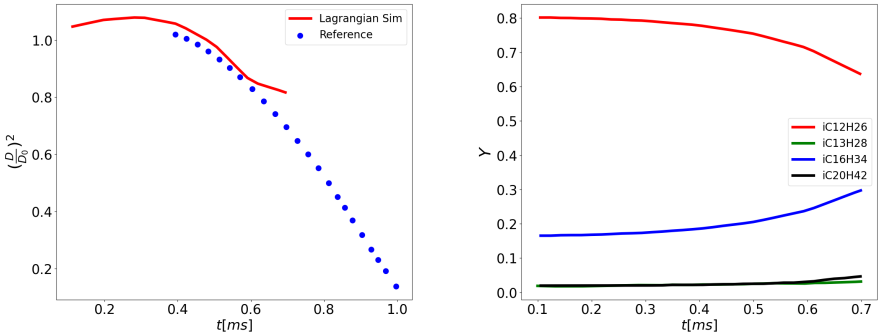

(b) T = 1200 K, P = 20 bar, Cruise CRZ

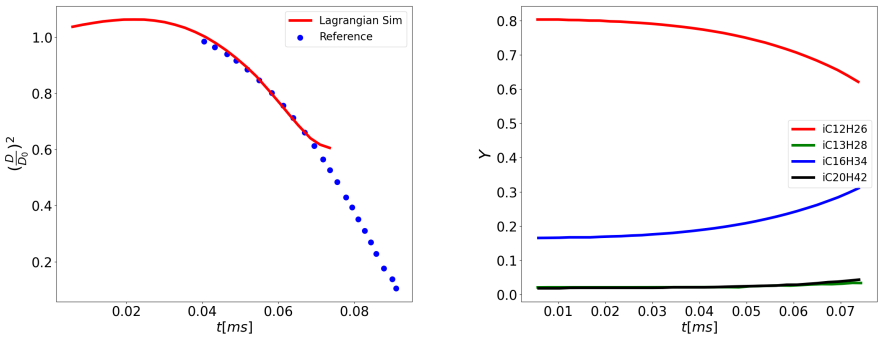

(c) T = 900 K, P = 60 bar, Takeoff ORZ

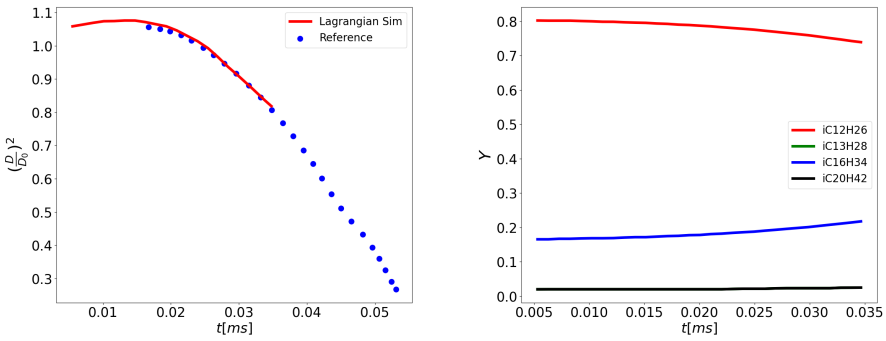

(d) T = 1200 K, P = 60 bar, Takeoff CRZ

Fig. 7 Evaporation characteristics of four-component SAF surrogate C1 for operating conditions mentioned in Table 2 (left). Variation of droplet composition (species mass fractions) during evaporation also shown (right). Comparison against data from Poblador-Ibanez et al. [45].

The preferential evaporation effect was also well captured in the C1 evaporation case, where the more volatile $iC_{12}H_{26}$ evaporated faster than the heavier $iC_{20}H_{42}$. The introduction of the heavier component results in an increase in the droplet lifetime, which is also well captured by the new model.

Acknowledgments

The submitted manuscript has been created by UChicago Argonne, LLC, Operator of Argonne National Laboratory ("Argonne"). Argonne, a U.S. Department of Energy Office of Science laboratory, is operated under Contract No. DE-AC02-06CH11357. The U.S. Government retains for itself, and others acting on its behalf, a paid-up nonexclusive, irrevocable worldwide license in said article to reproduce, prepare derivative works, distribute copies to the public, and perform publicly and display publicly, by or on behalf of the Government. The Department of Energy will provide public access to these results of federally sponsored research in accordance with the DOE Public Access Plan. http://energy.gov/downloads/doe-public-access-plan.

This work has been funded by the DOE Office of Energy Efficiency and Renewable Energy (EERE). The authors wish to thank Kevin Stork and Gurpreet Singh at the DOE Vehicle Technologies Office (VTO) for their support.

The authors thank the Laboratory Computing Resource Center (LCRC), who provided the clusters Bebop and Improv to allow for model development and CFD simulations.

S. Yang and N. Srinivasan gratefully acknowledge the support from the Office of Naval Research (ONR), under grant number N00014-22-1-2287 supervised by program officer Dr. Steven Martens. The views and conclusions contained herein are those of the authors only and should not be interpreted as representing those of ONR, the U.S. Navy or the U.S. Government.

References

[1] Kurzawska, P., "Overview of Sustainable Aviation Fuels including emission of particulate matter and harmful gaseous exhaust gas compounds," *Transportation Research Procedia*, Vol. 59, 2021, pp. 38–45. https://doi.org/10.1016/j.trpro.2021.11.095, 10th International Conference on Air Transport – INAIR 2021, TOWARDS AVIATION REVIVAL.

[2] Colket, M., Heyne, J., Rumizen, M., Gupta, M., Edwards, T., Roquemore, W. M., Andac, G., Boehm, R., Lovett, J., Williams, R., et al., "Overview of the national jet fuels combustion program," *AIAA Journal*, Vol. 55, No. 4, 2017, pp. 1087–1104. https://doi.org/10.2514/1.J055361.

[3] Kallupalayam Ramasamy, K., Thorson, M. R., Billing, J. M., Holladay, J. E., Drennan, C., Hoffman, B., and Haq, Z., "Hydrothermal Liquefaction: Path to Sustainable Aviation Fuel," Tech. rep., Pacific Northwest National Lab.(PNNL), Richland, WA (United States), 2021. https://doi.org/10.2172/1821809.

[4] Huber, M. L., Lemmon, E. W., and Bruno, T. J., "Surrogate mixture models for the thermophysical properties of aviation fuel Jet-A," *Energy & Fuels*, Vol. 24, No. 6, 2010, pp. 3565–3571. https://doi.org/10.1021/ef100208c.

[5] Dooley, S., Won, S. H., Chaos, M., Heyne, J., Ju, Y., Dryer, F. L., Kumar, K., Sung, C.-J., Wang, H., Oehlschlaeger, M. A., et al., "A jet fuel surrogate formulated by real fuel properties," *Combustion and Flame*, Vol. 157, No. 12, 2010, pp. 2333–2339. https://doi.org/10.1016/j.combustflame.2010.07.001.

[6] Jones, W., Marquis, A., and Vogiatzaki, K., "Large-eddy simulation of spray combustion in a gas turbine combustor," *Combustion and Flame*, Vol. 161, No. 1, 2014, pp. 222–239. https://doi.org/10.1016/j.combustflame.2013.07.016.

[7] Yang, V., "Modeling of supercritical vaporization, mixing, and combustion processes in liquid-fueled propulsion systems," *Proceedings of the Combustion Institute*, Vol. 28, No. 1, 2000, pp. 925–942. https://doi.org/10.1016/S0082-0784(00)80299-4.

[8] Van Konynenburg, P., and Scott, R., "Critical lines and phase equilibria in binary van der Waals mixtures," *Philosophical Transactions of the Royal Society of London. Series A, Mathematical and Physical Sciences*, Vol. 298, No. 1442, 1980, pp. 495–540. https://doi.org/10.1098/rsta.1980.0266.

[9] Zhang, H., Yi, P., and Yang, S., "Multicomponent Effects on the Supercritical CO2 Systems: Mixture Critical Point and Phase Separation," *Flow, Turbulence and Combustion*, Vol. 109, No. 2, 2022, pp. 515–543. https://doi.org/10.1007/s10494-022-00335-9.

[10] Srinivasan, N., Zhang, H., and Yang, S., "A VLE-Based Reacting Flow Solver for High-Pressure Transcritical Two-Phase Combustion," *AIAA SCITECH 2023 Forum*, 2023, p. 1858. https://doi.org/10.2514/6.2023-1858.

[11] Zhang, H., Srinivasan, N., and Yang, S., "In situ adaptive tabulation of vapor-liquid equilibrium solutions for multi-component high-pressure transcritical flows with phase change," *Journal of Computational Physics*, Vol. 500, 2024, p. 112752. https://doi.org/10.1016/j.jcp.2024.112752.

[12] Srinivasan, N., and Yang, S., "Artificial neural network aided vapor–liquid equilibrium model for multi-component high-pressure transcritical flows with phase change," *Physics of Fluids*, Vol. 36, 2024, p. 083328. https://doi.org/10.1063/5.0219323.

[13] Dasgupta, D., and Som, S., "Fuel Property Impact on Lean Blow Out for Sustainable Aviation Fuels in Gas Turbine Combustors," *Turbo Expo: Power for Land, Sea, and Air*, Vol. 87943, American Society of Mechanical Engineers, 2024, p. V03AT04A073. https://doi.org/10.1115/GT2024-126789.

[14] Mohaddes, D., Brouzet, D., and Ihme, M., "Cost-constrained adaptive simulations of transient spray combustion in a gas turbine combustor," *Combustion and Flame*, Vol. 249, 2023, p. 112530. https://doi.org/10.1016/j.combustflame.2022.112530.

[15] Crowe, C. T., *Multiphase Flow Handbook*, CRC press, 2005.

[16] Dukowicz, J. K., "A particle-fluid numerical model for liquid sprays," *Journal of Computational Physics*, Vol. 35, No. 2, 1980, pp. 229–253. https://doi.org/10.1016/0021-9991(80)90087-X.

[17] Keller, P., Knorsch, T., Wensing, M., and Hasse, C., "The influence of differential evaporation on the structure of a three-component biofuel spray," *International Journal of Engine Research*, Vol. 16, No. 5, 2015, pp. 610–626. https://doi.org/10.1177/1468087415573800.

[18] Burger, M., Schmehl, R., Prommersberger, K., Schäfer, O., Koch, R., and Wittig, S., "Droplet evaporation modeling by the distillation curve model: accounting for kerosene fuel and elevated pressures," *International Journal of Heat and Mass Transfer*, Vol. 46, No. 23, 2003, pp. 4403–4412. https://doi.org/10.1016/S0017-9310(03)00286-2.

[19] Foundation, T. O., *OpenFOAM-6*, www.openfoam.org, 2018.

[20] Poblador-Ibanez, J., and Nocivelli, L., "Toward a Real-Fluid Modeling Framework for Sustainable Aviation Fuels," *Fuel Communications*, Vol. 18, 2024, p. 100100. https://doi.org/10.1016/j.jfueco.2023.100100.

[21] Soave, G., "Equilibrium constants from a modified Redlich-Kwong equation of state," *Chemical Engineering Science*, Vol. 27, No. 6, 1972, pp. 1197–1203. https://doi.org/10.1016/0009-2509(72)80096-4.

[22] Peng, D.-Y., and Robinson, D. B., "A new two-constant equation of state," *Industrial & Engineering Chemistry Fundamentals*, Vol. 15, No. 1, 1976, pp. 59–64. https://doi.org/10.1021/i160057a011.

[23] Lin, H., and Duan, Y.-Y., "Empirical correction to the Peng–Robinson equation of state for the saturated region," *Fluid Phase Equilibria*, Vol. 233, No. 2, 2005, pp. 194–203. https://doi.org/10.1016/j.fluid.2005.05.008.

[24] Lin, H., Duan, Y.-Y., Zhang, T., and Huang, Z.-M., "Volumetric property improvement for the Soave- Redlich- Kwong equation of state," *Industrial & Engineering Chemistry Research*, Vol. 45, No. 5, 2006, pp. 1829–1839. https://doi.org/10.1021/ie051058v.

[25] Baled, H., Enick, R. M., Wu, Y., McHugh, M. A., Burgess, W., Tapriyal, D., and Morreale, B. D., "Prediction of hydrocarbon densities at extreme conditions using volume-translated SRK and PR equations of state fit to high temperature, high pressure PVT data," *Fluid Phase Equilibria*, Vol. 317, 2012, pp. 65–76. https://doi.org/10.1016/j.fluid.2011.12.027.

[26] Prausnitz, J. M., and Tavares, F. W., "Thermodynamics of fluid-phase equilibria for standard chemical engineering operations," *AIChE Journal*, Vol. 50, No. 4, 2004, pp. 739–761. https://doi.org/10.1002/aic.10069.

[27] Huber, M. L., Lemmon, E. W., Bell, I. H., and McLinden, M. O., "The NIST REFPROP database for highly accurate properties of industrially important fluids," *Industrial & Engineering Chemistry Research*, Vol. 61, No. 42, 2022, pp. 15449–15472. https://doi.org/10.1021/acs.iecr.2c01427.

[28] Boehm, R. C., Hauck, F., Yang, Z., Wanstall, C. T., and Heyne, J. S., "Error quantification of the Arrhenius blending rule for viscosity of hydrocarbon mixtures," *Frontiers in Energy Research*, Vol. 10, 2022, p. 1074699. https://doi.org/10.3389/fenrg.2022.1074699.

[29] Poling, B. E., Prausnitz, J. M., O'connell, J. P., et al., *The Properties of Gases and Liquids*, Vol. 5, Mcgraw-hill New York, 2001.

[30] Chung, T. H., Ajlan, M., Lee, L. L., and Starling, K. E., "Generalized multiparameter correlation for nonpolar and polar fluid transport properties," *Industrial & Engineering Chemistry Research*, Vol. 27, No. 4, 1988, pp. 671–679. https://doi.org/10.1021/ie00076a024.

[31] Richter, S., Kukkadapu, G., Westbrook, C. K., Braun-Unkhoff, M., Naumann, C., Köhler, M., and Riedel, U., "A combined experimental and modeling study of combustion properties of an isoparaffinic alcohol-to-jet fuel," *Combustion and Flame*, Vol. 240, 2022, p. 111994. https://doi.org/10.1016/j.combustflame.2022.111994.

[32] Luning Prak, D. J., Jones, M. H., Trulove, P., McDaniel, A. M., Dickerson, T., and Cowart, J. S., "Physical and chemical analysis of alcohol-to-jet (ATJ) fuel and development of surrogate fuel mixtures," *Energy & Fuels*, Vol. 29, No. 6, 2015, pp. 3760–3769. https://doi.org/10.1021/acs.energyfuels.5b00668.

[33] Nannoolal, Y., Rarey, J., and Ramjugernath, D., "Estimation of pure component properties: Part 2. Estimation of critical property data by group contribution," *Fluid Phase Equilibria*, Vol. 252, No. 1, 2007, pp. 1–27. https://doi.org/10.1016/j.fluid.2006.11.014.

[34] Tahami, S., Movagharnejad, K., and Ghasemitabar, H., "Estimation of the critical constants of organic compounds via a new group contribution method," *Fluid Phase Equilibria*, Vol. 494, 2019, pp. 45–60. https://doi.org/10.1016/j.fluid.2019.04.022.

[35] Muller, K., Mokrushina, L., and Arlt, W., "Second-order group contribution method for the determination of the dipole moment," *Journal of Chemical & Engineering Data*, Vol. 57, No. 4, 2012, pp. 1231–1236. https://doi.org/10.1021/je2013395.

[36] Greenshields, C., "Notes on Computational Fluid Dynamics: General Principles — doc.cfd.direct," https://doc.cfd.direct/notes/cfd-general-principles/the-pimple-algorithm, 2022.

[37] Kee, R. J., Rupley, F. M., Meeks, E., and Miller, J. A., "CHEMKIN-III: A FORTRAN chemical kinetics package for the analysis of gas-phase chemical and plasma kinetics," Tech. rep., Sandia National Lab.(SNL-CA), Livermore, CA (United States), 1996.

[38] Fuller, E. N., Schettler, P. D., and Giddings, J. C., "New method for prediction of binary gas-phase diffusion coefficients," *Industrial & Engineering Chemistry*, Vol. 58, No. 5, 1966, pp. 18–27. https://doi.org/10.1021/ie50677a007.

[39] Takahashi, S., "Preparation of a generalized chart for the diffusion coefficients of gases at high pressures," *Journal of Chemical Engineering of Japan*, Vol. 7, No. 6, 1975, pp. 417–420. https://doi.org/10.1252/jcej.7.417.

[40] Nguyen, D. N., Jung, K. S., Shim, J. W., and Yoo, C. S., "Real-fluid thermophysicalModels: An OpenFOAM-based library for reacting flow simulations at high pressure," *Computer Physics Communications*, Vol. 273, 2022, p. 108264. https://doi.org/10.1016/j.cpc.2021.108264.

[41] Fuchs, N. A., *Evaporation and Droplet Growth in Gaseous Media*, Elsevier, 2013.

[42] Bancroft, W. D., and Davis, H., "Raoult's Law." *The Journal of Physical Chemistry*, Vol. 33, No. 3, 2002, pp. 361–370. https://doi.org/10.1021/J150297A004.

[43] Nomura, H., Ujiie, Y., Rath, H. J., Sato, J., and Kono, M., "Experimental study on high-pressure droplet evaporation using microgravity conditions," *Symposium (International) on Combustion*, Vol. 26, Elsevier, 1996, pp. 1267–1273. https://doi.org/10.1016/S0082-0784(96)80344-4.

[44] Zhang, H., "Evaporation of a suspended droplet in forced convective high-pressure environments," *Combustion Science and Technology*, Vol. 175, No. 12, 2003, pp. 2237–2268. https://doi.org/10.1080/714923282.

[45] Poblador-Ibanez, J., Nocivelli, L., and Dasgupta, D., "Multi-component Evaporation of Sustainable Aviation Fuel Droplets," *AIAA SCITECH 2024 Forum*, 2024, p. 1997. https://doi.org/10.2514/6.2024-1997.

[46] Edwards, J. T., "Reference jet fuels for combustion testing," *55th AIAA Aerospace Sciences Meeting*, 2017, p. 0146. https://doi.org/10.2514/6.2017-0146.